

***Electronic Supplementary Information***

**Tuning the electrostatic energy landscape within the pores of covalent organic frameworks: post-synthetic modification reactions and structural imperfections**

Egbert Zojer

*Institute of Solid State Physics, NAWI Graz, Graz University of Technology, Petersgasse 16, A-8010 Graz, AUSTRIA*

*ORCID-ID: 0000-0002-6502-1721*

## S1. Details of the electrostatic model

The shift in electrostatic energy at point  $\vec{r}$  (denoted as  $\Delta E(\vec{r})$ ) induced by a point dipole,  $\vec{p}$ , at the origin is given by

$$\Delta E(\vec{r}) = \frac{-e}{4\pi\epsilon_0} \frac{\vec{p}\vec{r}}{r^3}. \quad (1)$$

For a series of dipoles characterized by two indices  $i, j$  at positions  $\vec{r}_{ij}$  this becomes

$$\Delta E(\vec{r}) = \sum_{ij} \frac{-e}{4\pi\epsilon_0} \frac{\vec{p}_{ij}(\vec{r}-\vec{r}_{ij})}{|\vec{r}-\vec{r}_{ij}|^3}. \quad (2)$$

Writing this expression cartesian coordinates and assuming that all dipoles  $\vec{p}_{ij}$  are within the xy plane one obtains:

$$\Delta E(x, y, z) = \sum_{ij} \frac{-e}{4\pi\epsilon_0} \frac{p_{ij}^x(x-r_{ij}^x)+p_{ij}^y(y-r_{ij}^y)}{\left((x-r_{ij}^x)^2+(y-r_{ij}^y)^2+(z-r_{ij}^z)^2\right)^{3/2}}. \quad (3)$$

Provided that the dipoles in the x,y plane are arranged on circles with radius R and that dipole moments are aligned radially pointing outside one obtains for the components and positions of the x- and y-components of the dipoles (provided that the absolute values of the dipole moments of all dipoles are identical amounting to p)

$$p_{ij}^x = p \cdot \cos(\phi_i); p_{ij}^y = p \cdot \sin(\phi_i); r_{ij}^x = R \cdot \cos(\phi_i); r_{ij}^y = R \cdot \sin(\phi_i), \quad (4)$$

with  $\phi_i$  representing the polar angle of dipole  $i, j$  assuming that the dipole orientation does not depend on index  $j$  (which will be the index denoting the individual layers stacked in z-direction in which the circles of dipoles are arranged). Inserting this into equation (3) yields

$$\Delta E(x, y, z) = \sum_{ij} \frac{-e}{4\pi\epsilon_0} \frac{p \cdot \cos(\phi_i)x + p \cdot \sin(\phi_i)y - p \cdot (\cos(\phi_i))^2 R - p \cdot (\sin(\phi_i))^2 R}{\left((x-R \cdot \cos(\phi_i))^2 + (y-R \cdot \sin(\phi_i))^2 + (z-j \cdot d)^2\right)^{3/2}} = \sum_{ij} \frac{-e}{4\pi\epsilon_0} \frac{p \cdot \cos(\phi_i)x + p \cdot \sin(\phi_i)y - p \cdot R}{\left((x-R \cdot \cos(\phi_i))^2 + (y-R \cdot \sin(\phi_i))^2 + (z-j \cdot d)^2\right)^{3/2}}. \quad (5)$$

For  $I$  equally spaced dipoles one each circle of dipoles and  $2J+1$  stacked dipole layers one gets the final equation for the perfectly ordered cylindrical arrangement of dipoles:

$$\Delta E(x, y, z) = \sum_{j=-J}^J \sum_{i=0}^I \frac{-e}{4\pi\epsilon_0} \frac{p \cdot \cos\left(\frac{i2\pi}{I}\right)x + p \cdot \sin\left(\frac{i2\pi}{I}\right)y - p \cdot R}{\left(\left(x-R \cdot \cos\left(\frac{i2\pi}{I}\right)\right)^2 + \left(y-R \cdot \sin\left(\frac{i2\pi}{I}\right)\right)^2 + (z-j \cdot d)^2\right)^{3/2}} \quad (6)$$

If consecutive layers are slipped relative to each other by a distance  $s$ , the following transition occurs:

$$r_{ij}^x = R \cdot \cos(\phi_i) \rightarrow r_{ij}^x = R \cdot \cos(\phi_i) + j \cdot s \quad (7)$$

This changes the expression for the shift in the electrostatic energy of an electron to:

$$\Delta E(x, y, z) = \sum_{j=-J}^J \sum_{i=0}^I \frac{-e}{4\pi\epsilon_0} \frac{p \cdot \cos\left(\frac{i \cdot 2\pi}{l}\right)(x-j \cdot s) + p \cdot \sin\left(\frac{i \cdot 2\pi}{l}\right)y - p \cdot R}{\left(\left(x-j \cdot s - R \cdot \cos\left(\frac{i \cdot 2\pi}{l}\right)\right)^2 + \left(y - R \cdot \sin\left(\frac{i \cdot 2\pi}{l}\right)\right)^2 + (z-j \cdot d)^2\right)^{3/2}}. \quad (8)$$

In case the magnitude of this displacement becomes random, one simply obtains

$$\Delta E(x, y, z) = \sum_{j=-J}^J \sum_{i=0}^I \frac{-e}{4\pi\epsilon_0} \frac{p \cdot \cos\left(\frac{i \cdot 2\pi}{l}\right)(x-\hat{A} \cdot s) + p \cdot \sin\left(\frac{i \cdot 2\pi}{l}\right)y - p \cdot R}{\left(\left(x-\hat{A} \cdot s - R \cdot \cos\left(\frac{i \cdot 2\pi}{l}\right)\right)^2 + \left(y - R \cdot \sin\left(\frac{i \cdot 2\pi}{l}\right)\right)^2 + (z-j \cdot d)^2\right)^{3/2}}, \quad (9)$$

with  $\hat{A}_j$  being a series of random numbers between -1 and 1. Finally, if not only the distances of the slips are random (determined by  $\hat{A}_j$ , now between 0 and 1), but also their directions (determined by a set of polar angles  $\hat{B}_j \cdot 2\pi$ , with  $\hat{B}_j$  between 0 and 1), one gets

$$\Delta E(x, y, z) = \sum_{j=-J}^J \sum_{i=0}^I \frac{-e}{4\pi\epsilon_0} \frac{p \cdot \cos\left(\frac{i \cdot 2\pi}{l}\right)(x-\hat{A} \cdot s \cdot \cos(\hat{B}_j \cdot 2\pi)) + p \cdot \sin\left(\frac{i \cdot 2\pi}{l}\right)(y-\hat{A} \cdot s \cdot \sin(\hat{B}_j \cdot 2\pi)) - p \cdot R}{\left(\left(x-\hat{A} \cdot s \cdot \cos(\hat{B}_j \cdot 2\pi) - R \cdot \cos\left(\frac{i \cdot 2\pi}{l}\right)\right)^2 + \left(y-\hat{A} \cdot s \cdot \sin(\hat{B}_j \cdot 2\pi) - R \cdot \sin\left(\frac{i \cdot 2\pi}{l}\right)\right)^2 + (z-j \cdot d)^2\right)^{3/2}}. \quad (10)$$

The above equations have been evaluated and plotted using the Mathematica 11.3<sup>38</sup> program suite. For plotting the potentials of quasi-infinitely extended extended stacks, 201 layers have been typically considered, for calculating the numerical value of the electrostatic energy in the pore center, in most cases 2001 layers were included, even though the resulting deviations compared to 201 layers were negligible.

## S2. Additional methodological details

The basis functions employed in the FHI-aims simulations have the format<sup>i</sup>

$$\Phi(r) = \frac{u(r)}{r} * Y_{lm}(\Theta, \Phi)$$

with  $u(r)$  being a predefined radial function and the  $Y_{lm}$  being spherical harmonics;  $r$ ,  $\Theta$ , and  $\Phi$  are spherical coordinates relative to a given atomic center. The details of the functions (including information on, e.g., integration grids, etc.) are provided in so-called *species\_defaults* files, which are shipped together with FHI-aims. Based on the convergence tests in [1], the predefined “tight” basis sets were employed without any further adjustments.

*Table S1. Details on the basis functions employed in FHI-aims calculations: The abbreviations read as follows:  $X(nl, z)$ , where  $X$  describes the type of basis function:  $H$  stands for hydrogen-like functions and*

<sup>i</sup> As described in the FHI-aims manual, version January 23, 2017.

ionic for a free-ion like radial function. The parameter  $n$  denotes the main/radial quantum number,  $l$  the angular momentum quantum number ( $s, p, d, f, \dots$ ), and  $z$  an effective nuclear charge. The latter for the hydrogen-like functions scales the radial function in the defining Coulomb potential. In the case of free-ion like radial functions,  $z$  specifies the onset radius of the confining potential. If *auto* is specified, the default onset is used.

	H	C	N	O	F
Minimal	valence (1s, 1.0)	valence (2s, 2.0)	valence (2s, 2.0)	valence (2s, 2.0)	valence (2s, 2.0)
	ion_occ (1s, 0.5)	valence (2p, 2.0)	valence (2p, 3.0)	valence (2p, 4.0)	valence (2p, 5.0)
		ion_occ (2s, 2.0)	ion_occ (2s, 1.0)	ion_occ (2s, 1.0)	ion_occ (2s, 1.0)
		ion_occ (2p, 2.0)	ion_occ (2p, 2.0)	ion_occ (2p, 3.0)	ion_occ (2p, 4.0)
First tier	H(2s, 2.1)	H(2p, 1.7)	H(2p, 1.8)	H(2p, 1.8)	H(2p, 1.7)
	H(2p, 3.5)	H(3d, 6)	H(3d, 6.8)	H(3d, 7.6)	H(3d, 4.7)
		H(2s, 4.9)	H(3s, 5.8)	H(3s, 6.4)	H(3s, 6.8)
Second tier	H(1s, 0.85)	H(4f, 9.8)	H(4f, 10.8)	H(4f, 11.6)	H(4f, 11.2)
	H(2p, 3.7)	H(3p, 5.2)	H(3p, 5.8)	H(3p, 6.2)	Ionic (2p,auto)
	H(2s, 1.2)	H(3s, 4.3)	H(1s, 0.8)	H(3d, 5.6)	H(1s, 0.75)
	H(3d, 7.0)	H(5g, 14.4)	H(5g, 16)	H(5g, 17.6)	H(4d, 8..8)
		H(3d, 6.2)	H(3d, 4.9)	H(1s, 0.75)	H(5g, 16.8)

The convergence criteria for the self-consistency cycle were set to the default values for changes in the charge density ( $10^{-5}$ ), in the total energy ( $10^{-6}$  eV), and in the forces ( $10^{-4}$  eV·Å<sup>-1</sup>). To describe the occupation of the Kohn-Sham eigenstates, a Gaussian broadening function with a width of  $s = 0.01$  eV was used and relativistic effects were accounted for by the atomic ZORA approximation.<sup>64</sup>

To determine changes in electrostatic energy via electrostatic core-level shifts, probe atoms were placed at specific positions and the shifts in their core-level energies were analysed. To eliminate the simultaneous occurrence of chemical shifts, inert (Ne) atoms were chosen as these probe particles. They were placed at the centres of the channels and in vacuum 30 Å above the topmost layers of the finite-thickness slabs described in the manuscript. In this setup, the differences in electrostatic energy between the two locations can be determined simply from difference of the respective Ne-1s core-level energies. The position of the vacuum level was determined by systematically changing the isovalue in a plot of the Hartree energy and eventually choosing the value at which the respective contour plots would extend most strongly into the vacuum region between periodic replicas of the slab.

Plots of the MOF geometries and isovalue plots of the electrostatic energy were produced using OVITO<sup>2</sup>; cross-sections illustrating the electrostatic energies in specific planes were plotted using VESTA;<sup>3</sup> The structures overlaid on the cross-sections of the electrostatic energies were produced using OVITO. MarvinSketch was used for drawing, chemical structures, ChemAxon (<https://www.chemaxon.com>)

### **S3. Structural properties of the COFs and COF slabs**

The structures of all systems were optimized using the algorithm and convergence criterion listed in the main manuscript. When optimizing stacks slipped in the same direction, the unit cell contained one monolayer, in the case of alternately slipped cells, two monolayers needed to be included. Geometry optimizations were typically started from two differently slipped cells (one slipped in substituent direction and one slipped close to wall direction) and unless otherwise stated all geometric parameters were optimized. In most instances, both optimizations converged into the same structure. In case this strategy yielded two different conformations with reasonably similar geometries, these are listed separately below and corresponding datapoints are included in the relevant plots of the main manuscript. To ensure that none of the geometry optimizations had ended in a saddle point, it would have been ideal to also calculate vibrational frequencies, respectively phonon bands to identify non-stable unit cells. This is, however, beyond what can be done for systems of the size and multitude studied here. Nevertheless, the author is confident that at least local minimum structures were reached judging from the convergence behaviour of the optimizations starting from two initial structures, which often involved massive changes in the unit cell geometries and, moreover, in the majority of the cases ended in the same structure. The following tables contain (i) all relevant unit cell parameters for the different studied variants of CPAE-CN (Table S2) (ii) and the most relevant unit-cell parameters for all optimized systems. As a general observation, slip distance are typically larger for more bulky and more polar substituents.

Table S2: Unit cells and relative energies of CPAE-CN type COFs.  $d$  denotes the distance between consecutive layers of the COFs (i.e., the component of the  $\mathbf{a}_3$  vector of the unit cell perpendicular to the plane defined by  $\mathbf{a}_1$  and  $\mathbf{a}_2$ ) and  $s$  is the magnitude of the slip of consecutive layers (i.e., the component of the  $\mathbf{a}_3$  vector parallel to the plane defined by  $\mathbf{a}_1$  and  $\mathbf{a}_2$ ); in analogy to the definition of spherical coordinates,  $\Theta$  refers to the angle between the  $\mathbf{a}_3$  vector and the normal to the  $(\mathbf{a}_1, \mathbf{a}_2)$  plane and  $\Phi$  denotes the angle between the projection of  $\mathbf{a}_3$  onto the  $(\mathbf{a}_1, \mathbf{a}_2)$  plane and the  $\mathbf{a}_1$  vector. For polymorphs with two layers in the unit cell,  $d$ ,  $s$ ,  $\Theta$ , and  $\Phi$  are specified not only for the whole unit cell, but also for the centres of consecutive layers.

name	$a_1/\text{\AA}$	$a_2/\text{\AA}$	$a_3/\text{\AA}$	$\langle \mathbf{a}_1, \mathbf{a}_2 \rangle /^\circ$	$\langle \mathbf{a}_1, \mathbf{a}_3 \rangle /^\circ$	$\langle \mathbf{a}_2, \mathbf{a}_3 \rangle /^\circ$	$d/\text{\AA}$	$s/\text{\AA}$	$\Theta/^\circ$	$\Phi/^\circ$
CPAE-CN	25.05	25.00	4.48	120.1	48.9	109.1	3.38	2.94	41.1	0.2
CPAE-CN*	25.03	25.02	5.01	120.0	46.4	125.9	3.35	3.72	48.1	22.0
CPAE/2-CN	25.04	25.00	6.68	120.1	90.0	90.1	6.68	0.04	0.10	83.9
between layers							3.34	2.89	41.0	1.0
CPAE/2-CN*	25.05	25.01	6.91	120.0	86.0	104.7	6.67	1.82	15.2	74.6
between layers							3.39	3.68	47.4	22.5

name	$\Delta \epsilon_{\text{layer}} / \text{meV}$	$\Delta \epsilon_{\text{subst}} / \text{meV}$	$\Delta \epsilon_{\text{atom}} / \text{meV}$
CPAE-CN	24	4	0.3
CPAE-CN*	0	0	0
CPAE/2-CN	105	18	1.2
CPAE/2-CN*	86	14	1.0

Table S3: geometrical parameters of the optimized structures of the 25 chemically different systems discussed in that paper.  $d$  denotes the distance between consecutive layers of the COFs (i.e., the component of the  $\mathbf{a}_3$  vector of the unit cell perpendicular to the plane defined by  $\mathbf{a}_1$  and  $\mathbf{a}_2$ ) and  $s$  is the magnitude of the slip of consecutive layers (i.e., the component of the  $\mathbf{a}_3$  vector of the unit cell parallel to the plane defined by  $\mathbf{a}_1$  and  $\mathbf{a}_2$ ); in analogy to the definition of spherical coordinates,  $\Theta$  refers to the angle between the  $\mathbf{a}_3$  vector and the normal to the  $(\mathbf{a}_1, \mathbf{a}_2)$  plane and  $\Phi$  denotes the angle between the projection of  $\mathbf{a}_3$  onto the  $(\mathbf{a}_1, \mathbf{a}_2)$  plane and the  $\mathbf{a}_1$  vector. As far as the directions of the slips of consecutive layers are concerned, due to the symmetry of the system, angles of  $0^\circ$ ,  $60^\circ$ ,  $120^\circ$ , ... correspond to slips in directions parallel to one of the substituent axes, angles of  $30^\circ$ ,  $90^\circ$ ,  $150^\circ$ , ... correspond to slips parallel to one the linker axes. The color code in the following table, denotes the conformation of the COF with green indicating slips largely in one of the substitution directions, red denoting slips in one of the linker directions and yellow highlighting slip directions in between (typically closer to one of the linker directions). When specifying the relative energetics, UC refers to unit cell and

*SUB to polar substituent. In case different conformations were found, they are reported provided that their energies were within 10 eV per unit cell.*

name	d / Å	s / Å	\Theta  / °	\Phi  / °	
<b>CPAE-CN (I)</b>	<b>3.38</b>	<b>2.94</b>	<b>41.1</b>	<b>0.2</b>	<b>slipped in substituent direction; higher in energy by 24 meV per UC (=0.3 meV/atom; =4.0 meV per SUB)<sup>1</sup></b>
<b>CPAE-CN* (I*)</b>	<b>3.35</b>	<b>3.72</b>	<b>48.1</b>	<b>22.0</b>	<b>slipped primarily in linker direction<sup>1</sup></b>
CPAE-(CN) <sub>5</sub> H <sub>1</sub>	3.35	2.92	41.2	0.1	slipped in direction of two -CN groups
CPAE-(CN) <sub>4</sub> H <sub>2</sub>	3.32	2.90	41.2	1.6	slipped in direction of two -CN groups
CPAE-(CN) <sub>3</sub> H <sub>3</sub>	3.31	2.75	39.8	0.1	slipped    to one -CN and one -H atom
CPAE-(CN) <sub>2</sub> H <sub>4</sub> *	3.32	2.47	36.8	1.4	slipped in direction of two H atoms; higher in energy by 15 meV per UC (=0.2 meV/atom; =2.5 meV per SUB) <sup>1</sup>
CPAE-(CN) <sub>2</sub> H <sub>4</sub>	3.37	1.71	27.0	0.3	slipped in direction of two H atoms
CPAE-(CN) <sub>1</sub> H <sub>5</sub>	3.37	1.67	26.4	0.1	slipped in direction of two H atoms
<b>CPAE-H (II)</b>	<b>3.38</b>	<b>1.62</b>	<b>25.8</b>	<b>0.0</b>	
<b>CPAE-F (III)</b>	<b>2.26</b>	<b>1.56</b>	<b>25.1</b>	<b>0.0</b>	
CPAE-F <sub>5</sub> H <sub>1</sub>	3.37	1.56	25.0	1.0	slipped in direction of two -F atoms
CPAE-F <sub>4</sub> H <sub>2</sub>	3.37	1.58	25.2	1.5	slipped in direction of two -F atoms
CPAE-F <sub>3</sub> H <sub>3</sub>	3.37	1.59	25.4	0.1	slipped in direction of one -F and one -H
CPAE-F <sub>2</sub> H <sub>4</sub>	3.37	1.60	25.5	1.5	slipped in direction of two -H atoms
CPAE-F <sub>1</sub> H <sub>5</sub>	3.37	1.61	25.6	0.7	slipped in direction of two -H atoms
<b>CPAE-NH<sub>2</sub> (IV)</b>	<b>3.31</b>	<b>1.48</b>	<b>24.0</b>	<b>1.6</b>	<b>higher in energy by 8 meV per UC (=0.1 meV/atom; =1.3 meV per SUB)<sup>1,2</sup></b>
<b>CPAE-NH<sub>2</sub>* (IV*)</b>	<b>3.30</b>	<b>1.51</b>	<b>24.5</b>	<b>34.0</b>	<b>slipped in linker direction<sup>1,2</sup></b>
CPAE-(NH <sub>2</sub> ) <sub>4</sub> H <sub>2</sub>	3.34	1.54	24.9	60.1	slipped in direction of two -H atoms <sup>3</sup>
CPAE-(NH <sub>2</sub> ) <sub>2</sub> H <sub>4</sub>	3.36	2.58	35.2	61.4	slipped in direction of two -H atoms <sup>4</sup>
<b>CPAE-CONH<sub>2</sub> (V)</b>	<b>3.13</b>	<b>3.83</b>	<b>50.9</b>	<b>0.5</b>	<sup>2</sup>
<b>CPAE-CONH<sub>2</sub>* (V*)</b>	<b>3.16</b>	<b>3.57</b>	<b>48.6</b>	<b>13.0<sup>5</sup></b>	<b>higher in energy by 701 meV per UC (=6.4 meV/atom; =117 meV per SUB)<sup>2</sup></b>
CPAE-(CONH <sub>2</sub> ) <sub>4</sub> (CN) <sub>2</sub>	3.27	3.64	48.4	42.4	<sup>2</sup>
CPAE-(CONH <sub>2</sub> ) <sub>2</sub> (CN) <sub>4</sub>	3.31	3.72	48.4	38.4	<sup>2</sup>
<b>CPAE-C(NO<sub>2</sub>)NH<sub>2</sub> (VI)</b>	<b>3.30</b>	<b>4.57</b>	<b>54.2</b>	<b>20.6</b>	
<b>CPAE-COOH (VII)</b>	<b>3.47</b>	<b>2.95</b>	<b>40.5</b>	<b>0.1</b>	
<b>CPAE-CH<sub>2</sub>NH<sub>2</sub> (VIII)</b>	<b>3.18</b>	<b>3.60</b>	<b>48.6</b>	<b>13.9</b>	<b>slip closer to substituent axis</b>
<b>CPAE-CH<sub>2</sub>NH<sub>2</sub>* (VIII*)</b>	<b>3.08</b>	<b>4.35</b>	<b>54.8</b>	<b>17.7</b>	<b>higher in energy by 138 meV per UC (=1.2 meV/atom; =23.0 meV per SUB)</b>
<b>CPAE-CH<sub>2</sub>N(CH<sub>3</sub>)<sub>2</sub> (IX)</b>	<b>3.22</b>	<b>2.88</b>	<b>42.0</b>	<b>23.7</b>	<b>geometry rather distorted</b>
CPAE-CH <sub>2</sub> (N(CH <sub>3</sub> ) <sub>2</sub> ) <sub>4</sub> (CN) <sub>2</sub>	3.42	2.71	38.6	59.9	slipped in direction of two -H atoms <sup>3</sup>

CPAE- <chem>CH2(N(CH3)2)2(CN)4</chem>	3.35	2.86	40.6	4.5	slipped in direction of two -H atoms
--	------	------	------	-----	--------------------------------------

<sup>1</sup> In these cases, the two COF conformations are essentially isoenergetic.

<sup>2</sup> H-bonding between substituents clearly relevant;

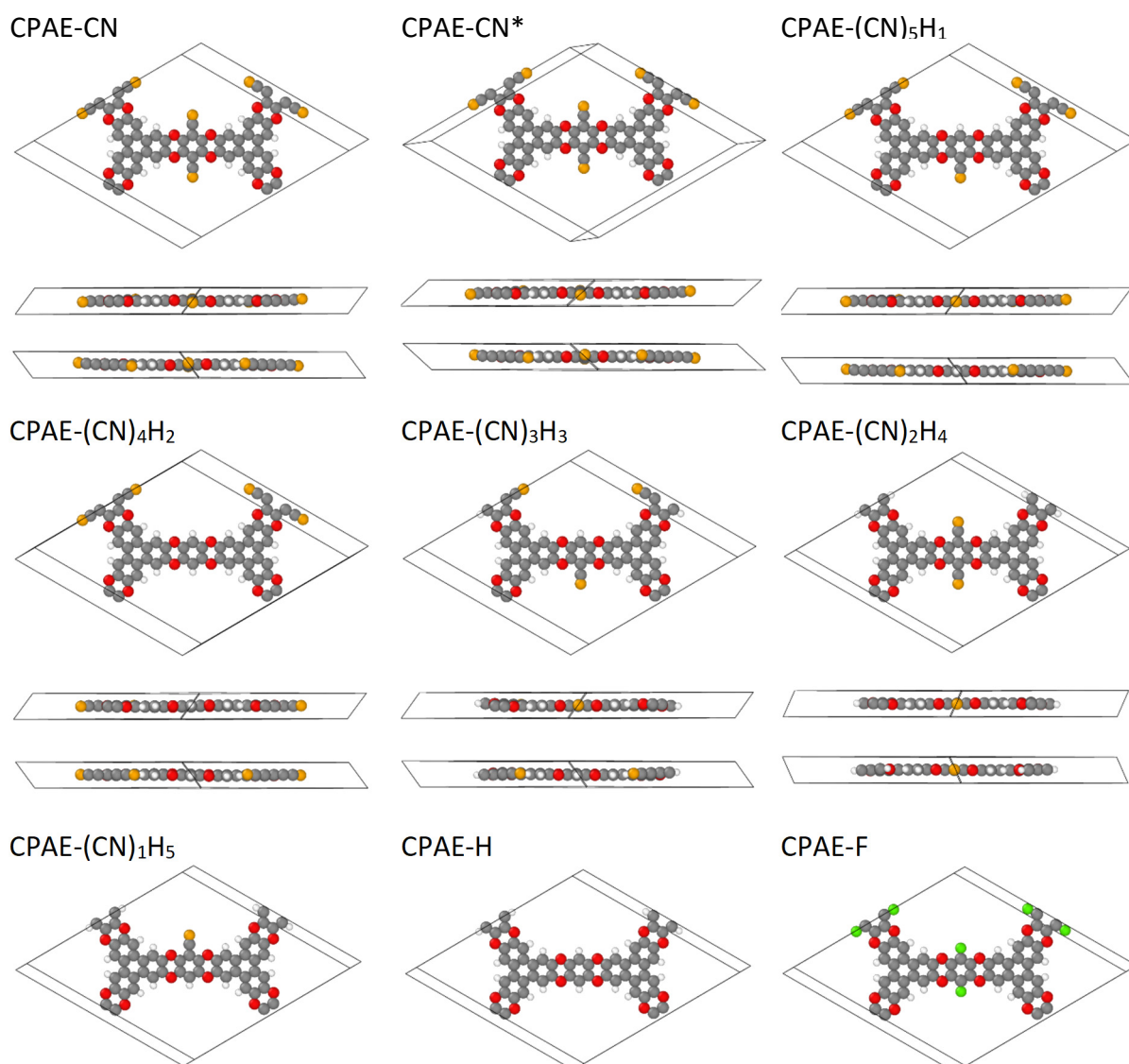
<sup>3</sup> direction of slip rotated during geometry optimization: starting geometry – slip in -NH<sub>2</sub> (CH<sub>2</sub>N(CH<sub>3</sub>)<sub>2</sub>) direction; final geometry in -H direction

<sup>4</sup> the reason for the change in  $\Phi$  during the geometry optimization from  $\sim 0^\circ$  to  $\sim 60^\circ$  was the alignment of the (somewhat pyramidal) -NH<sub>2</sub> groups, which for  $\Phi = \sim 60^\circ$  resulted in more efficient H-bonding.

<sup>5</sup> note that this angle is comparable to  $\Phi$  in the next two systems, as  $\Phi$ -angles for homogeneously substituted systems are defined only module  $60^\circ$  and positive and negative angles are equivalent.

## S4. Figures illustrating structural details of the studied systems

Several aspects discussed in the main manuscript are a consequence of the specific structures of certain COFs. Therefore, this section contains several figures, providing an overview of the optimised structures (Figure S1) and highlight specific structural details (Figure S2- Figure S6) mentioned in the main manuscript.



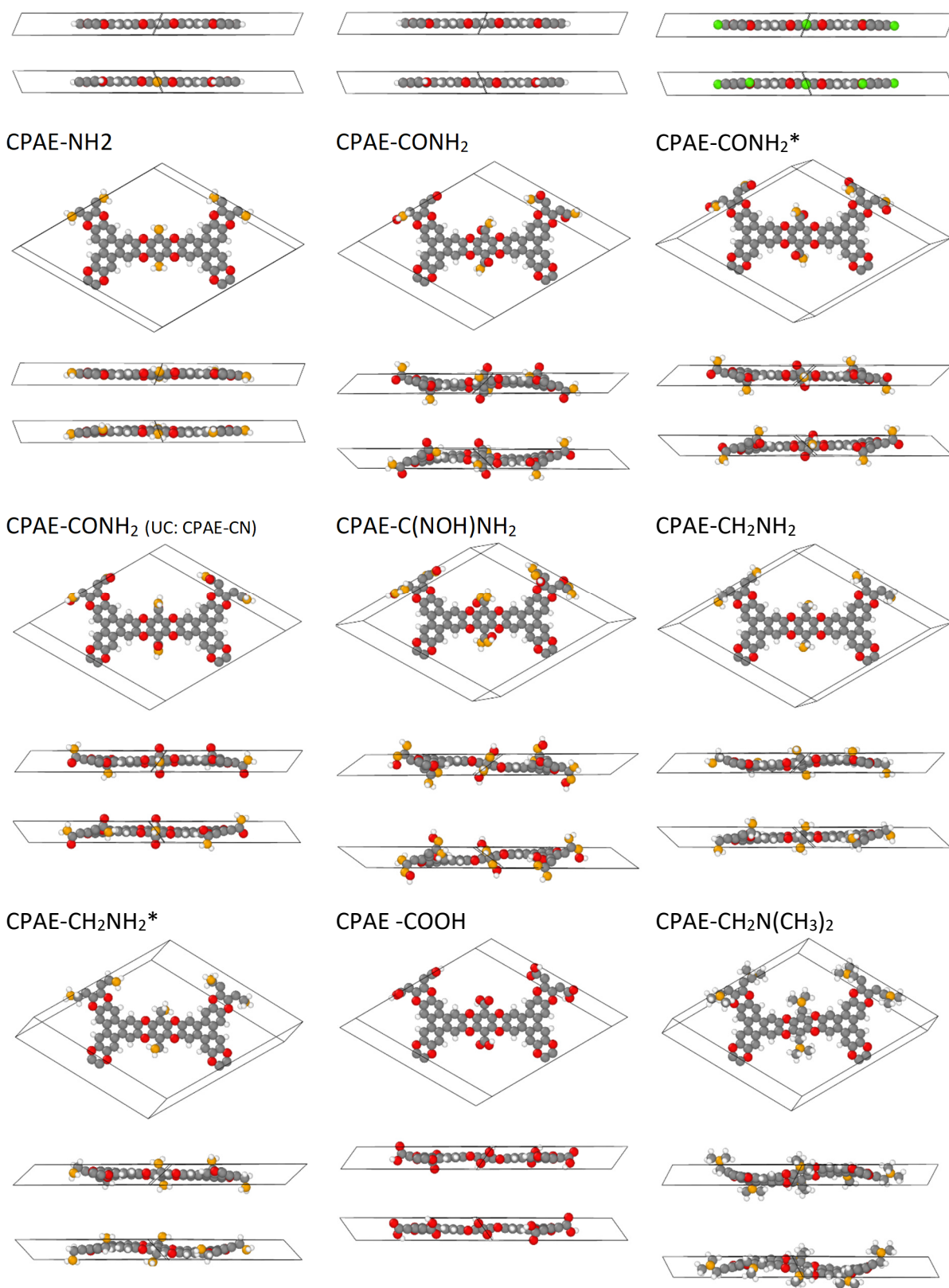


Figure S1: Optimized unit cells (including atoms forming the basis) of the most relevant structures of the materials studied here; the top panels show a top-view of the unit cell, followed by front- and a back-view. For CPAE-CONH<sub>2</sub> also the structure optimized with unit-cell parameters obtained in the CPAE-CN optimization is shown. colour code: grey: C, white: H, red: O, and orange: N, green: F.

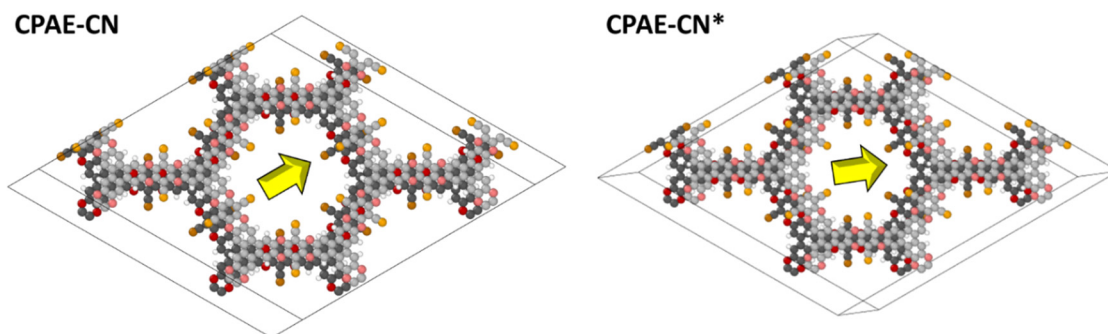


Figure S2:  $2 \times 2 \times 2$  supercells of CPAE-CN and CPAE-CN\* illustrating the difference in the slips between consecutive COF layers. The direction of the slip is also indicated by the arrows. colour code: grey: C, white: H, red: O, and orange: N, the atoms in the bottom layers are darker than the atoms in the top layers.

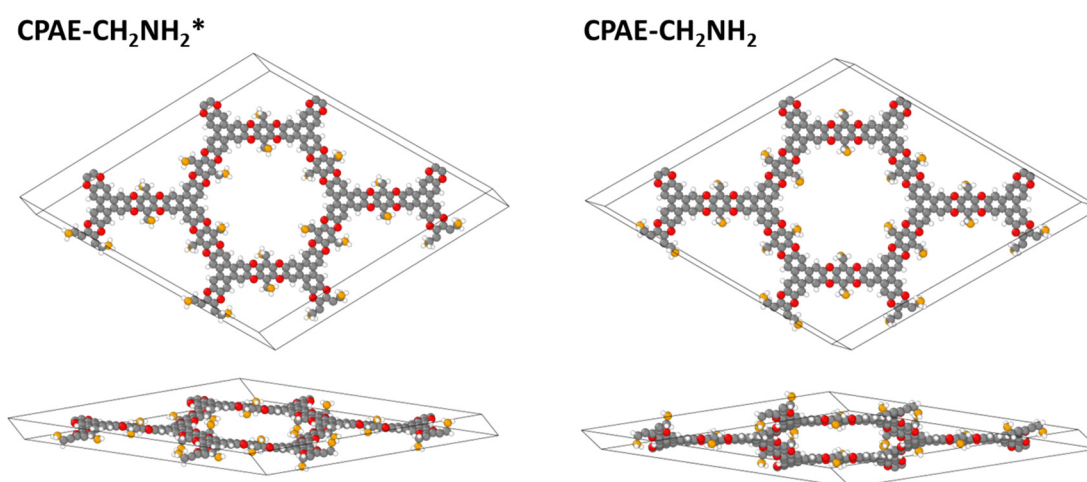


Figure S3:  $2 \times 2 \times 1$  supercells of CPAE-CH<sub>2</sub>NH<sub>2</sub> and CH<sub>2</sub>NH<sub>2</sub>\* illustrating the different orientations of the N-H bonds in the NH<sub>2</sub> groups contained in these systems. colour code: grey: C, white: H, red: O, and orange: N

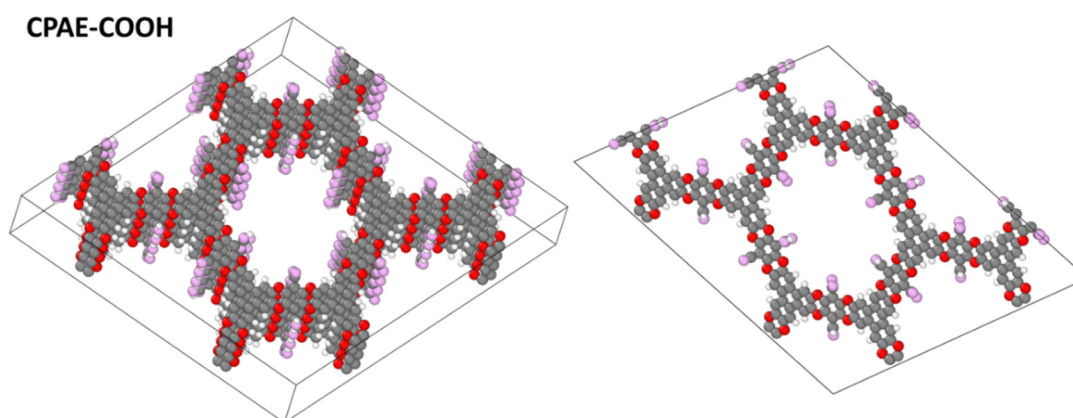


Figure S4:  $2 \times 2 \times 1$  supercells of CPAE-COOH illustrating the formation of H-bonded stripes of -COOH groups. In the right panel the viewing direction is along the stripes. colour code: grey: C, white: H, red: O, for better visibility, the O atoms in the -COOH groups are coloured in pink.

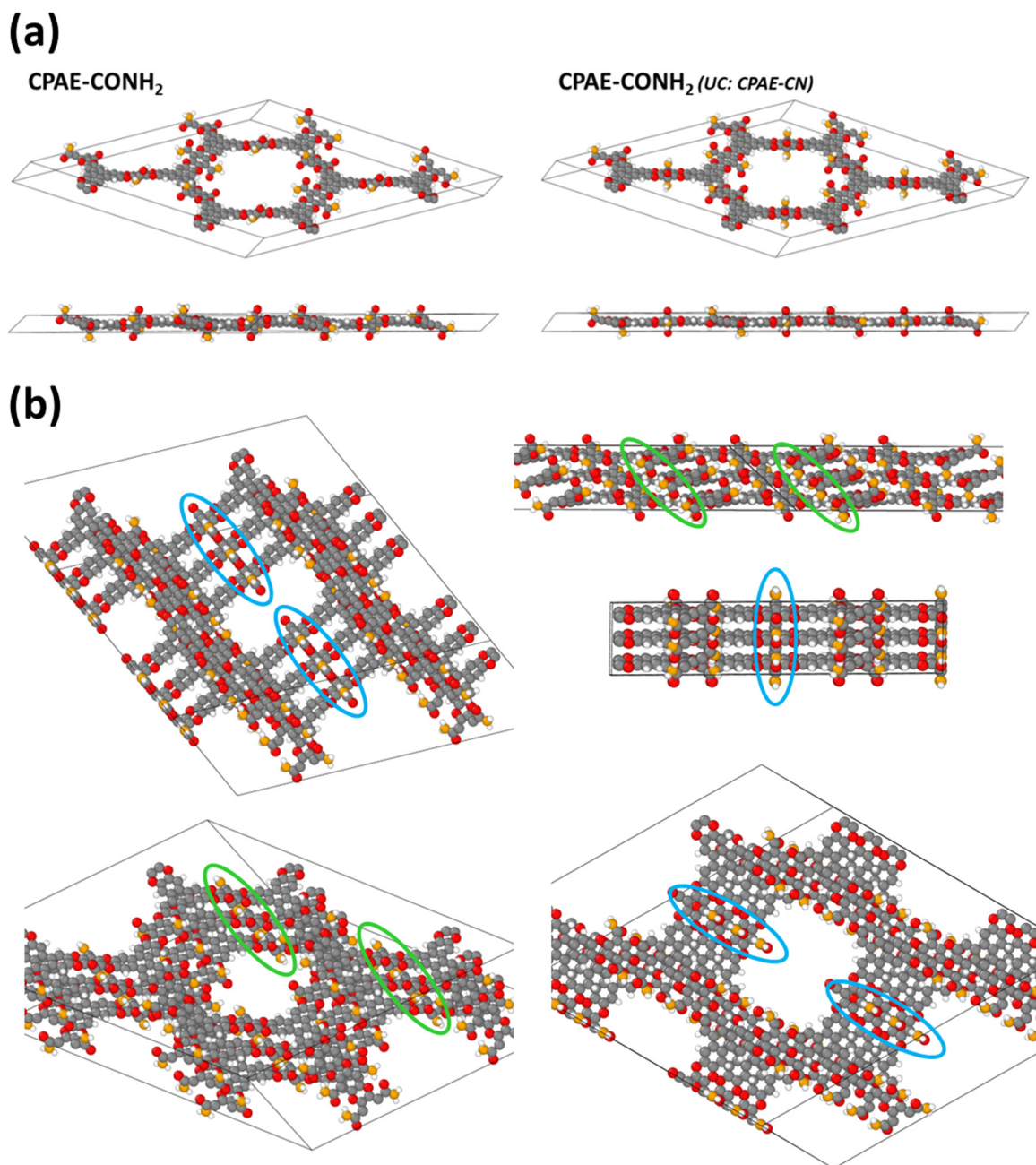


Figure S5: (a)  $2 \times 2 \times 1$  supercells of CPAE-CONH<sub>2</sub> illustrating the differences between the fully optimized structure (left) and the structure optimized fixing the unit-cell parameters to those obtained for CPAE-CN. (b) different views of a  $2 \times 2 \times 1$  supercell for the fully optimized structure to illustrate that for the -CONH<sub>2</sub> groups in slip direction the (C,O,N) planes are perpendicular to the planes of the COFs (selected examples highlighted by blue ellipses), while they are inclined for the other substituents (selected examples highlighted by green ellipses). The figures also shows, how the specific conformations of the substituents cause a distortion of the COF-backbones. colour code: grey: C, white: H, red: O.

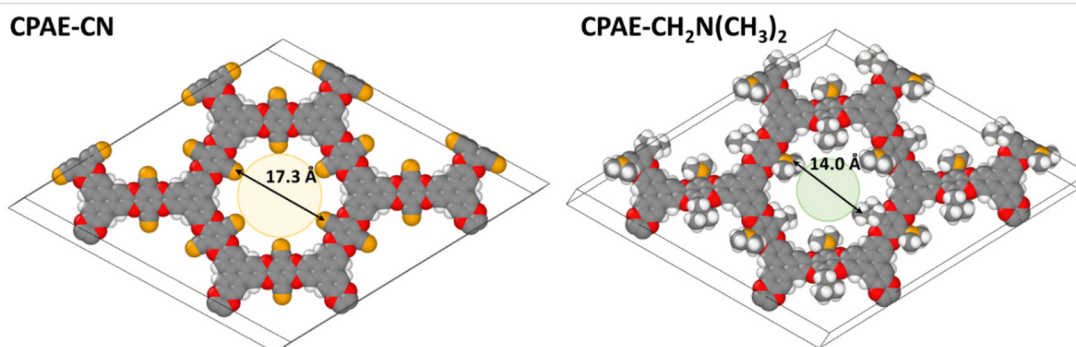


Figure S6:  $2 \times 2 \times 1$  supercells of CPAE-CN and CPAE-CH<sub>2</sub>N(CH<sub>3</sub>)<sub>2</sub> illustrating the reduction of the pore diameter in the latter system. For this plot, the radii of the spheres representing the atoms have been set to the respective van der Waals radii. The shortest distances between non-H atoms across the pores are indicated, where it should be mentioned that for ... The deviation of the atomic positions from the average plane of the COF-layer is no longer negligible. The orange and green circles are guides to the eye representing the largest circles that can be fitted into the projected structures of the COF layers.

## S5. Additional Data on the Electronic properties of the studied COFs and COF-slabs

Typically, in the main manuscript the electronic properties of fully optimized COF structures are discussed for which also the unit-cell parameters are optimized. Only when dealing with heterostructures, the structures of all sub-systems are confined to the unit-cell parameters of the CPAE-CN COF. Thus, in the following table, the shift in electrostatic energies in the pores relative to the vacuum level are compared for both types of geometries. The differences never exceed 0.1 eV.

Table S4: Shift between electrostatic energy in the center of the pore of an 11-layer stack and in vacuum. The shifts calculated for fully optimized structures (see Table S3) and structures optimized for fixed unit cell dimensions taken from CPAE-CN are compared (for details see main manuscript).

Name	optimized: $\Delta E_{\text{pore}} / \text{eV}$	UC of CPAE-CN: $\Delta E_{\text{pore}} / \text{eV}$
CPAE-CN (I)	0.93	
CPAE-CN* (I*)	0.77	
CPAE-(CN) <sub>3</sub> H <sub>3</sub>	0.45	0.42
CPAE-H (II)	-0.27	-0.20
CPAE-F (III)	0.19	0.14
CPAE-NH <sub>2</sub> (IV)	-0.38	-0.31
CPAE-CONH <sub>2</sub> (V)	-0.88	-0.78
CPAE-C(NO <sub>2</sub> )NH <sub>2</sub> (VI)	0.01	0.04

CPAE-COOH (VII)	0.34	0.34
CPAE-CH <sub>2</sub> NH <sub>2</sub> (VIII)	0.55	0.55
CPAE-CH <sub>2</sub> NH <sub>2</sub> * (VIII*)	-0.63	-0.72
CPAE-CH <sub>2</sub> N(CH <sub>3</sub> ) <sub>2</sub> (IX)	-0.29	-0.27

Plots of the electrostatic energy for the CPAE-CN structure are shown in panels (d)-(e) of Figure 3.

Equivalent plots for the alternately slipped system CPAE/2-CN are contained in the following graph.

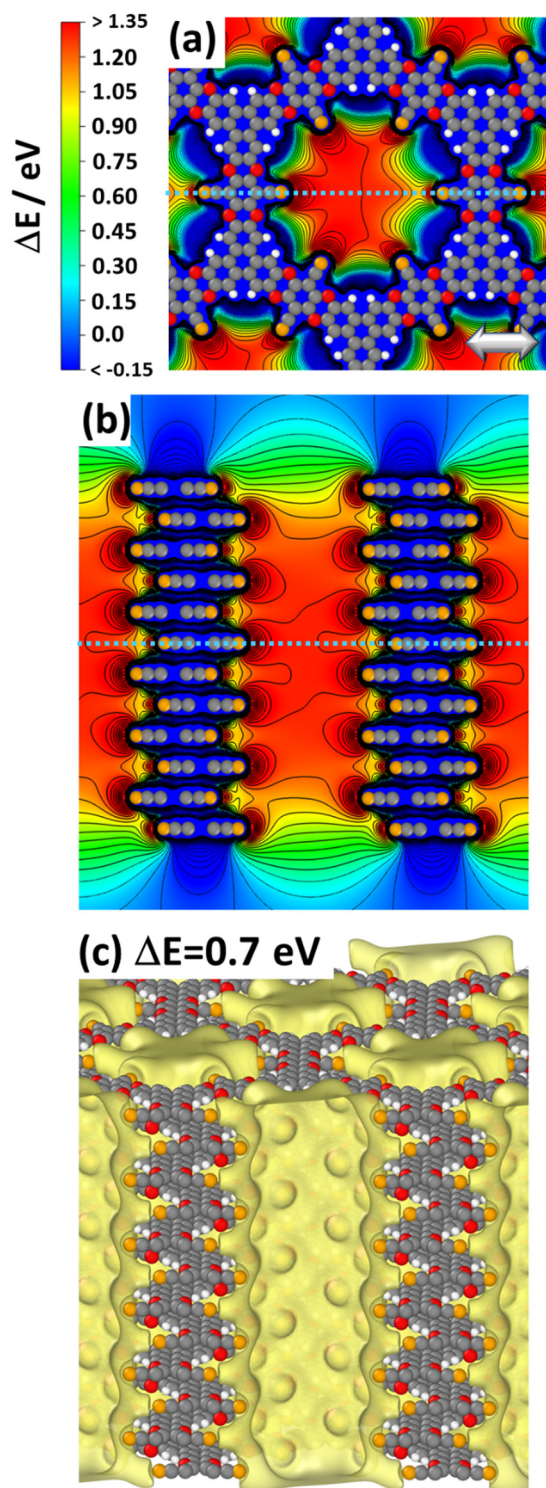


Figure S7: DFT-calculated electrostatic energies of an electron relative to the vacuum level,  $\Delta E$ , for the 12-layer slab of CPAE/2-CN for a cross-sections parallel to the (001) planes through the centre of the 7<sup>th</sup> layer of the slabs (as indicated by the dotted bright-blue lines in panel (b)). Panels (b) shows a cross-section parallel to the (010) plane containing the pore axis (indicated by dotted bright-blue line in panel (a)). Isolines are drawn every 0.1 eV and cover  $\Delta E$  values between -3.0 eV and the maximum values of  $\Delta E$ . Structures of individual COF layers, respectively of atoms essentially coinciding with the planes parallel to (010) through the COF centres are superimposed on the plots of the electrostatic energy as guides to the eye. The light grey double headed arrows in panel (a) indicates the slip direction of consecutive layers. Panels (c) shows an isovalue plots of  $\Delta E$  at values of 0.7 eV. I.e., within the region enclosed by the yellow isosurface the electrostatic energy is at least 0.7 eV higher than 30 Å above the topmost COF layer. colour code - grey: C orange: N, red: O; white: H; plots produced using OVITO<sup>44</sup> and VESTA<sup>68</sup>).

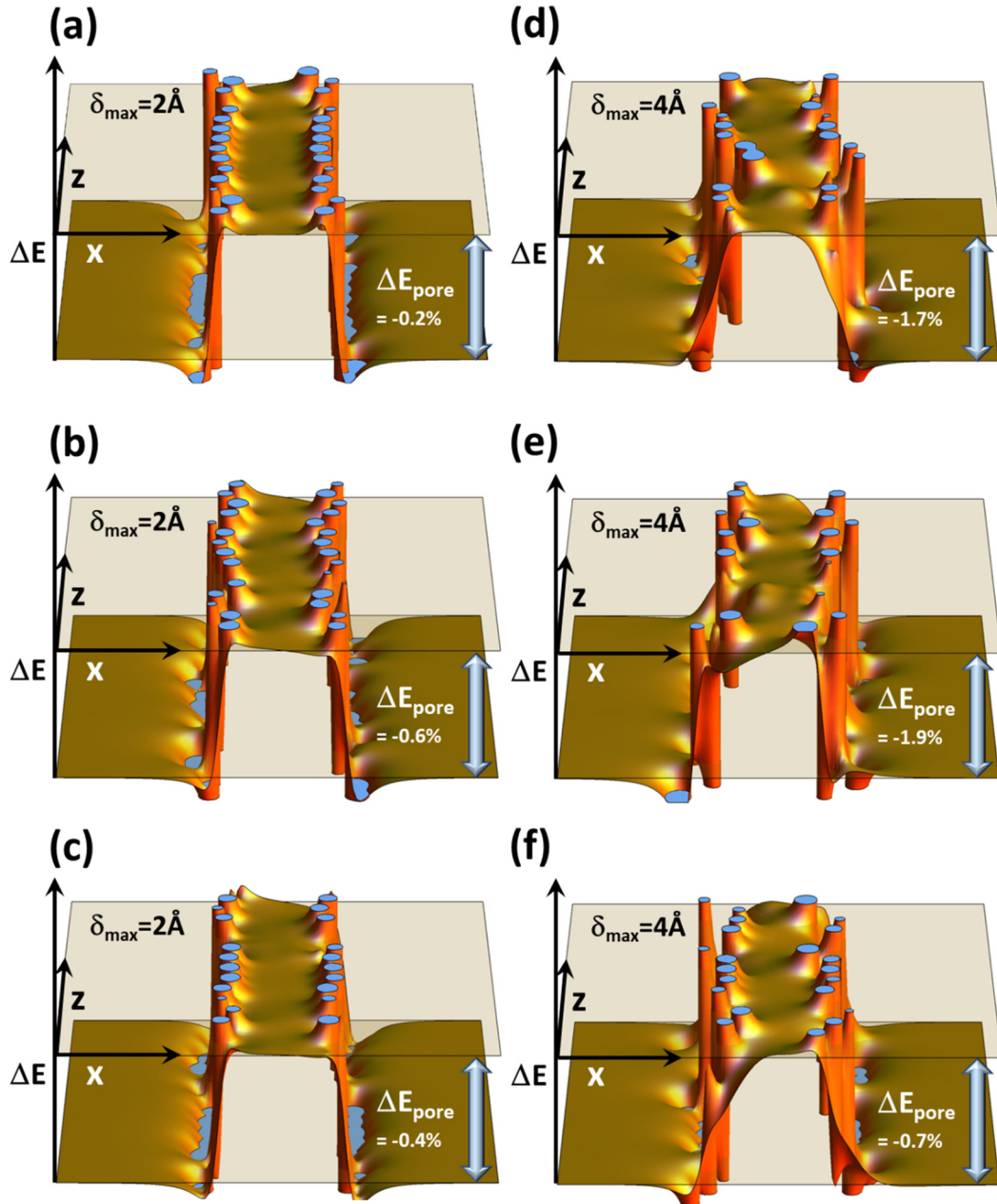


Figure S8: Shift in electrostatic energy obtained with the electrostatic model comprising 6 dipoles per layer (c.f., Figure 1(b)) for slips between consecutive layers that occur in random directions and by random magnitudes up to 2 Å in (a), (b), and (c) and up to 4 Å in (d), (e), and (f). The maximum slips correspond to half of the inter-layer spacing and the full inter-layer spacing assumed in the model. The diameter of the circle on which the dipoles are arranged amounts to  $27/\pi$  Å. The relative decrease of  $\Delta E_{\text{pore}}$  compared to the perfectly periodic eclipsed stack from Figure 1(f) is included in the plots after the  $\Delta E_{\text{pore}}$  label.

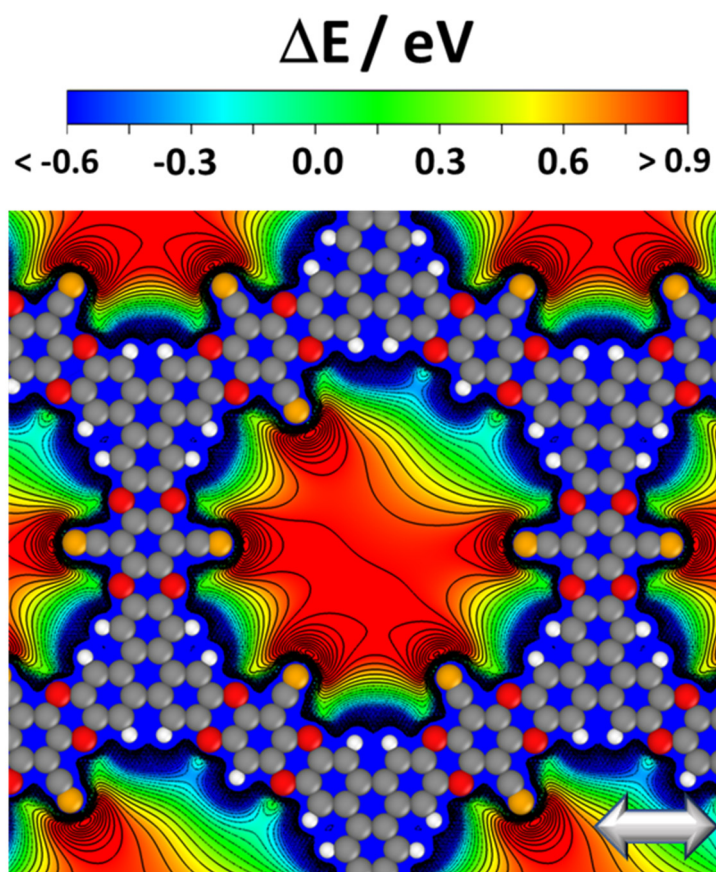


Figure S9: DFT-calculated electrostatic energy in an 11-layer stack of CPAE-CN in which one of the -CN groups in the central layer has been replaced by -H. The structures of an individual COF layer is superimposed on the plot of the electrostatic energy as guide to the eye. The light grey double headed arrow indicates the slip direction of consecutive layers. colour code - grey: C orange: N, red: O; white: H; plots produced using OVITO<sup>44</sup> and VESTA<sup>68</sup>).

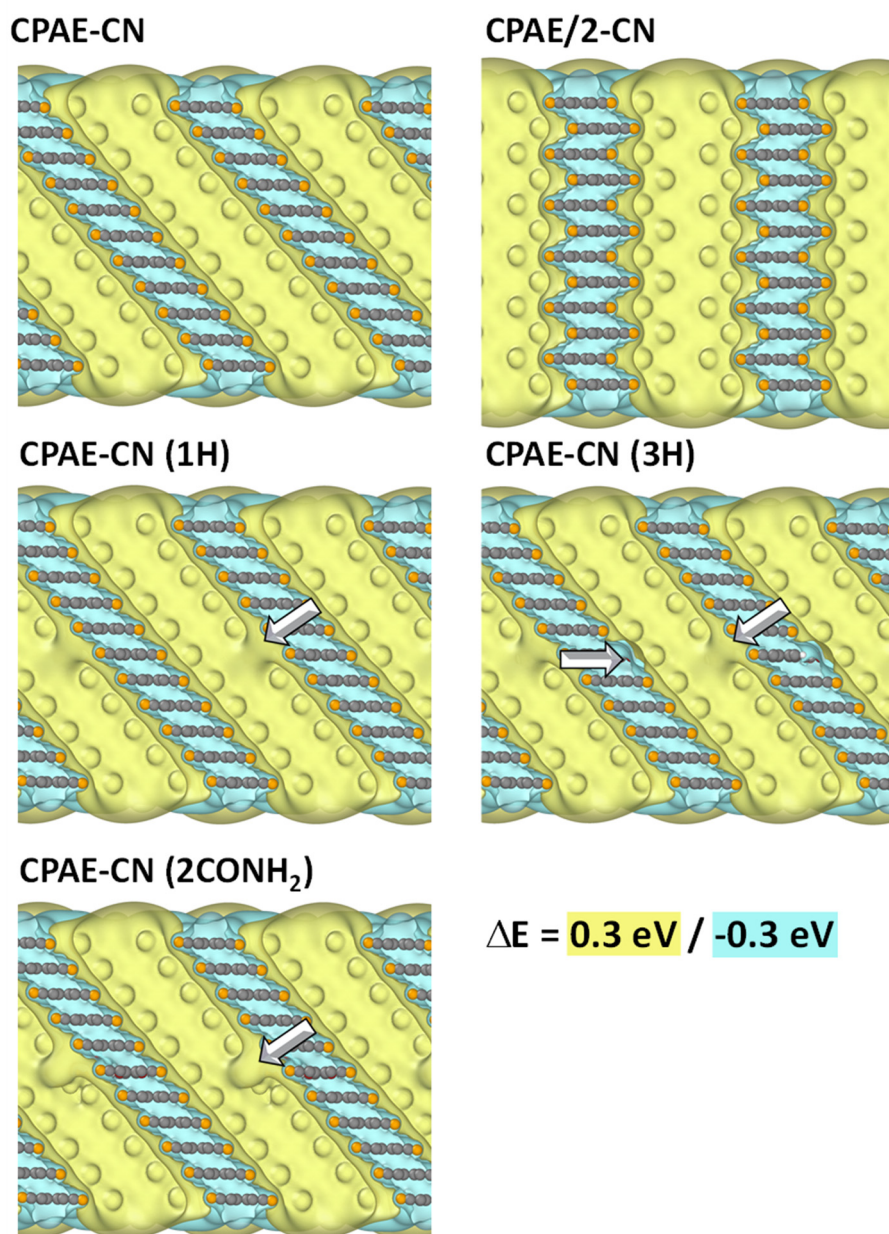


Figure S10: Isovalue plots for the electrostatic energy in 11-layer stacks of defect-free CPAE-CN (top two panels) and of CPAE-CN with one or three H substituents in the central layer (middle panels) and with two -CONH<sub>2</sub> defects in the middle layer (bottom panel). The yellow and blue isosurfaces denote energies of +0.3 eV and of -0.3 eV.

Figure 6 in the main manuscript contains cross-sections of the electrostatic energy for selected post-synthetically modified COFs. In Figure S11, equivalent plots are shown for the remaining systems.

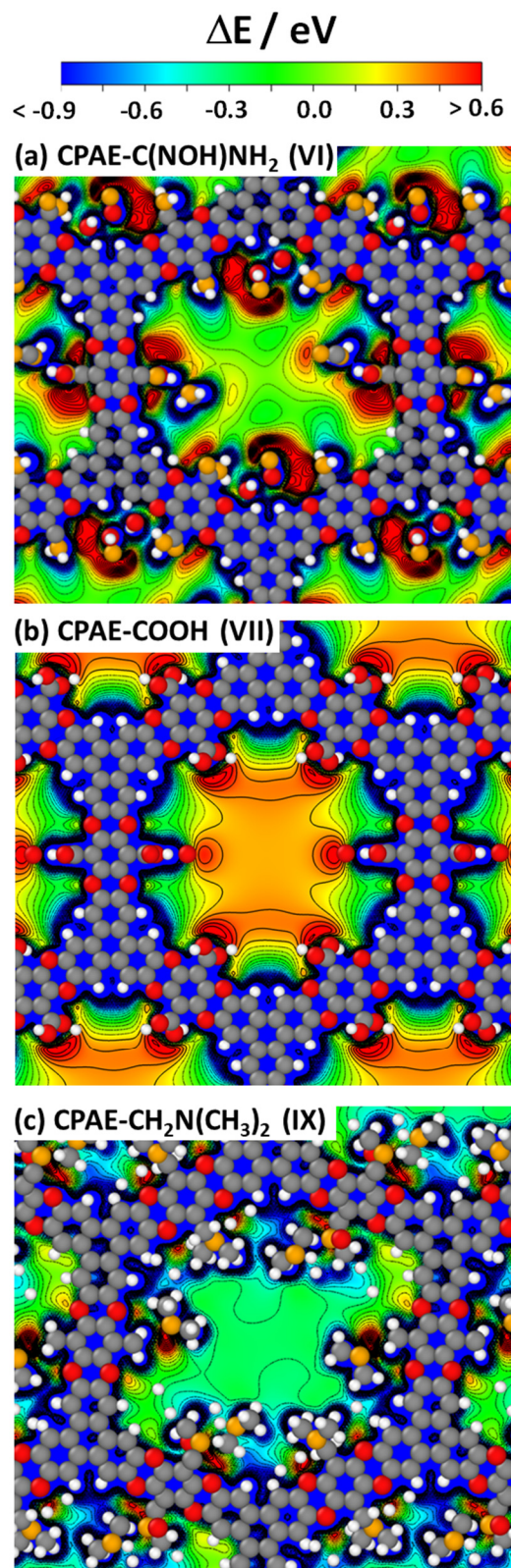


Figure S11: Electrostatic energies of electrons relative to the vacuum level,  $\Delta E$ , at the average height of the central layers of 11-layer stacks of the COFs indicated in the top-left corners of the panels. The colour/energy scale is provided at the top of the plot. The structures of the COFs are overlaid on the energy plots as a guide to the eye. As the individual layers of the COFs strongly deviate from planarity

(regarding the orientations of the substituents and/or the COF layers themselves) the overlaid structures do not correspond to individual monolayers, but comprise all atoms within  $\pm 2 \text{ \AA}$  of the plane for which the electrostatic energy is plotted. Isolines are drawn every 0.1 eV between to the maximum energy in the plane and an energy 3.0 eV below the vacuum level (notably, the electrostatic energy in the vicinity of the nuclei drops to much lower values).

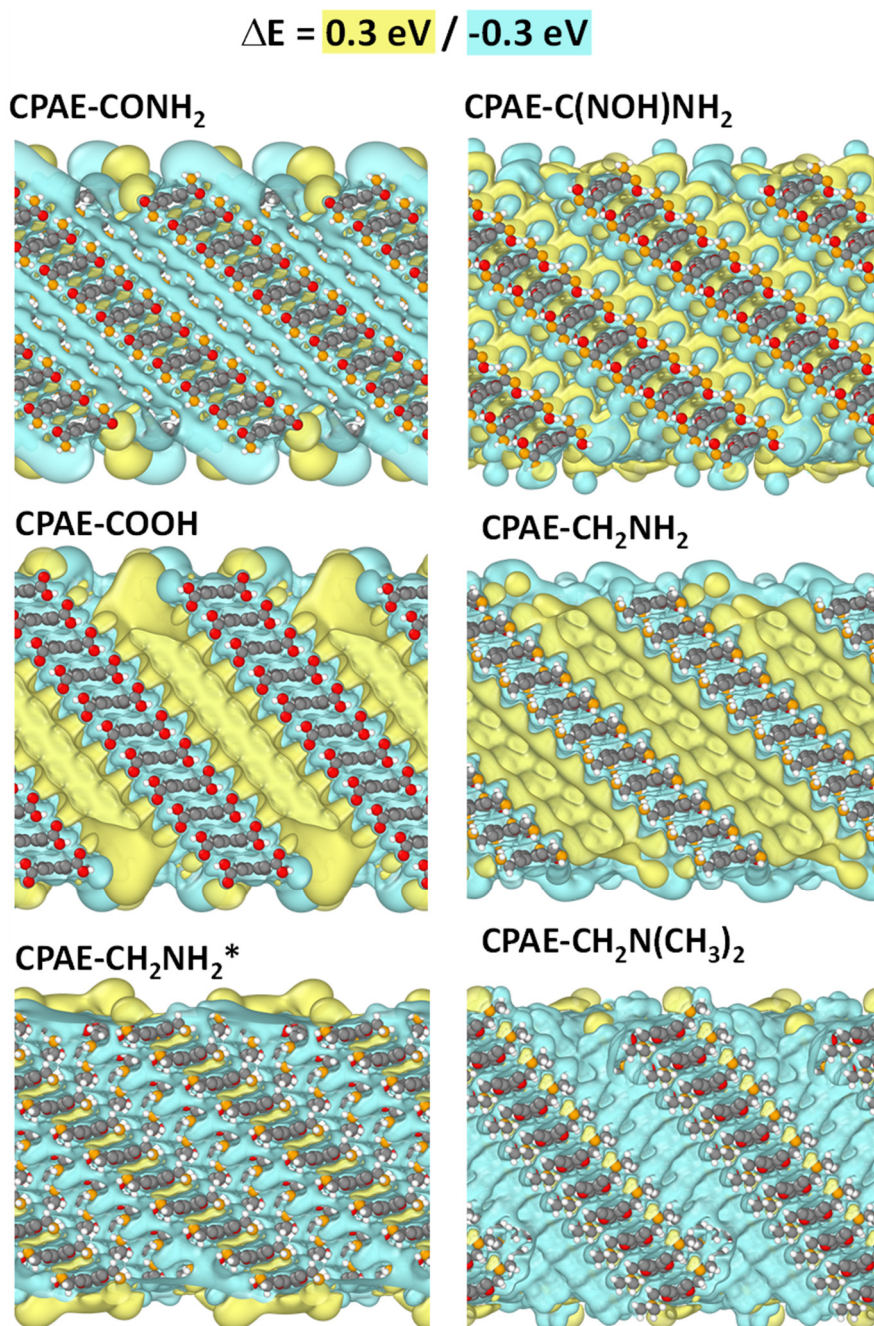


Figure S12: Isovalue plots for the electrostatic energy in 11-layer stacks of various post-synthetically modified CPAE-CN COFs. The yellow and blue isosurfaces denote energies of +0.3 eV and of -0.3 eV.

The main manuscript contains plots of  $\Delta E$  along the pore centres for COF heterostructures. In the following, corresponding plots for CPAE-CN and CPAE/2-CN are shown. They show that the shift in electrostatic energy slightly increases towards the centre of CPAE/2-CN in analogy to the situation observed for DUT-77 in [1]. Conversely, for CPAE-CN the maximum values of  $\Delta E$  are reached closer to the surface of the slabs. This is attributed to the different arrangement of the dipoles in the COFs with continuously slipped layers.

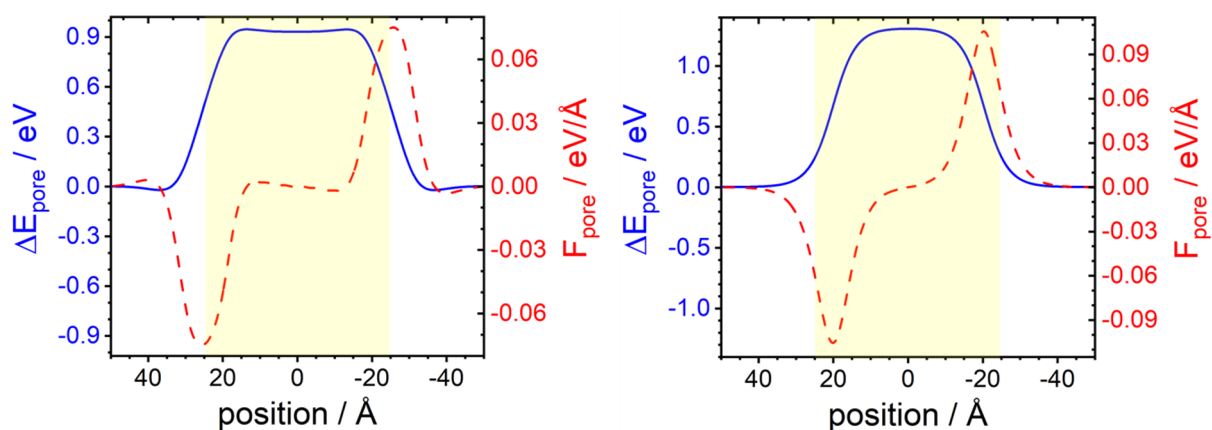


Figure S13: blue: Electrostatic energy of an electron,  $\Delta E_{\text{pore}}$ , along the centre of the pore relative to the electrostatic energy in vacuum for an 11-layer slab of CPAE-CN (top) and CPAE/2-CN red: derivative of the energy with respect to position (i.e., electrostatic force acting on an electron,  $F_{\text{pore}}$ ). A negative value of the  $F$  refers to a force acting from left to right (i.e., in the direction of a decreasing value of the position relative to the centre of the slab) for a negative charge and from right to left for a positive charge. The yellow shaded rectangles illustrate the region within the pores (set to the average positions of the top and bottom layers +  $\frac{1}{2}$  times the inter-layer distance).

The following plot contains isovalue plots of the CPAE-CN variants and of defective COFs that show both positive as well as negative values of the electrostatic energy. In Figure S9, equivalent plots for the post-synthetically modified COFs are shown, while Figure S10 contains such plots for the heterostructures.

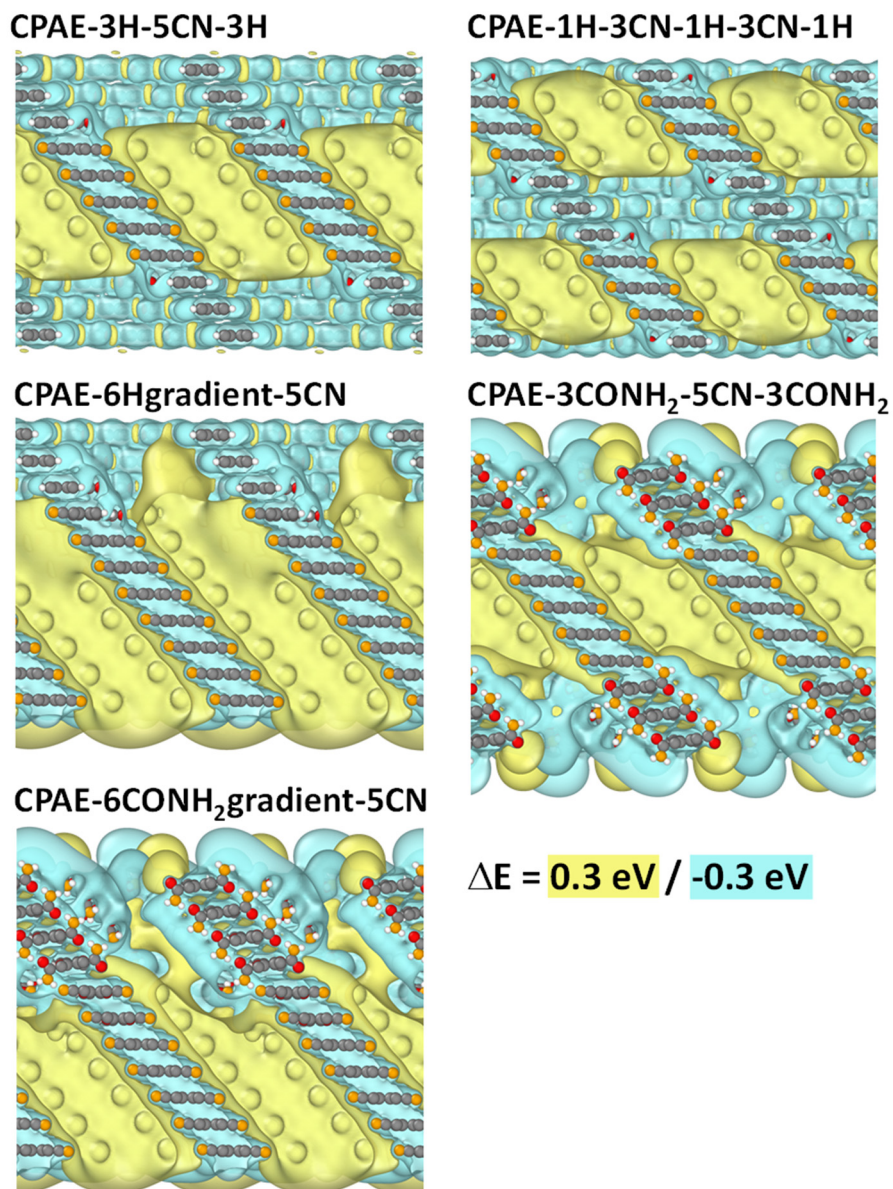


Figure S14: Isovalue plots for the electrostatic energy in 11-layer stacks consisting of various heterostructures. In the top-left panel, five CPAE-CN layers are sandwiched between two sets of three CPAE-H layers; in the top right panel, the situation for one CPAE-H layer followed by three CPAE-CN layers, three CPAE-H layers, three CPAE-CN layers, and one CPAE-layer is shown. The central, left panel illustrates five CPAE-CN layers covered by 6 layers with an increasing number of H-substituents (one H-defect up to six H-defects (i.e. CPAE-H)). The central right panel shows five CPAE-CN layers sandwiched between two sets of three CPAE-CONH<sub>2</sub> layers and the bottom-left panel is again a gradient structure in which the bottom five CPAE-CN layers are followed by three pairs of layers comprising two, four, and six -CONH<sub>2</sub> substituents. The yellow and blue isosurfaces denote energies of +0.3 eV and of -0.3 eV.

In Figure 6 of the main manuscript, the evolution of DE along the pore axis is shown for heterostructures containing hydrogenated COFs. Figure S12 provides such plots for CPAE-CONH<sub>2</sub> containing layers (including a gradient system); additionally, isovalue plots are shown, where Figure S12a is also contained in Figure 6 and is contained here only for the sake of comparison.

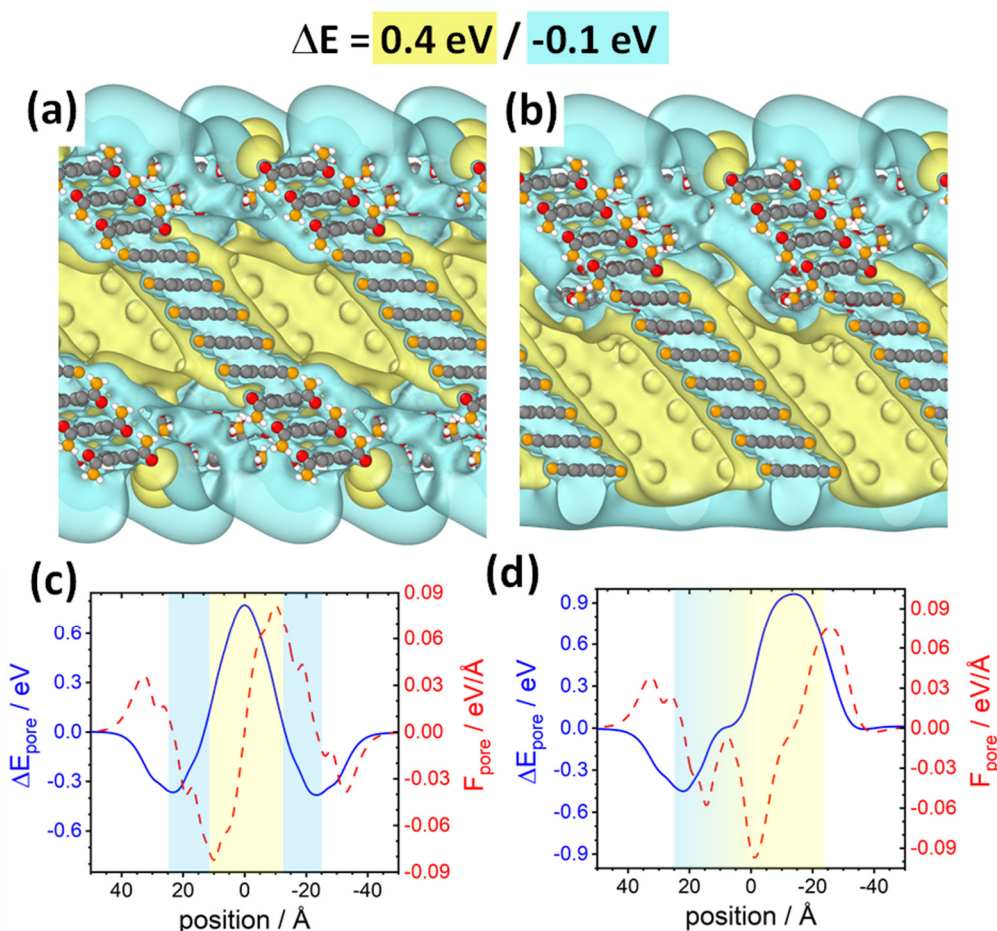


Figure S15: top panels: Isovalue plots for the electrostatic energy in 11-layer stacks consisting of five CPAE-CN layers sandwiched between two sets of three CPAE-CONH<sub>2</sub> layers (a) a gradient structure in which the bottom five CPAE-CN layers are followed by three pairs of layers comprising two, four, and six -CONH<sub>2</sub> substituents (b). In contrast to Figure S10, The yellow and blue isosurfaces denote energies of +0.4 eV and of -0.1 eV in analogy to Figure 6 of the main manuscript; bottom panels: electrostatic energies of an electron,  $\Delta E_{\text{pore}}$ , along the centre of the pore relative to the electrostatic energy in vacuum for the same heterostructures as in the top panels; red: derivative of the energy with respect to position (i.e., electrostatic force acting on an electron,  $F_{\text{pore}}$ ). A negative value of the  $F$  refers to a force acting from left to right (i.e., in the direction of a decreasing value of the position relative to the centre of the slab) for a negative charge and from right to left for a positive charge. The yellow shaded areas illustrate the region within the pores with (predominantly) -CN substituents, while the blue areas denote the regions with (predominantly) -CONH<sub>2</sub> substituents. The boundaries are aligned with the

average positions of the top and bottom layers of the respective regions +  $\frac{1}{2}$  times the inter-layer distance.

## S6. Properties of a Polar COFs with extended linkers

In the main manuscript, a system has been discussed, whose linkers contained each contained two -CN groups (one per pore bordered by the linker). To illustrate the generality of the described concept, also a system with four -CN groups per linker was investigated, which in the following will be referred to as COF-2CN. The structure of this system is compared to the original one in Figure S16.

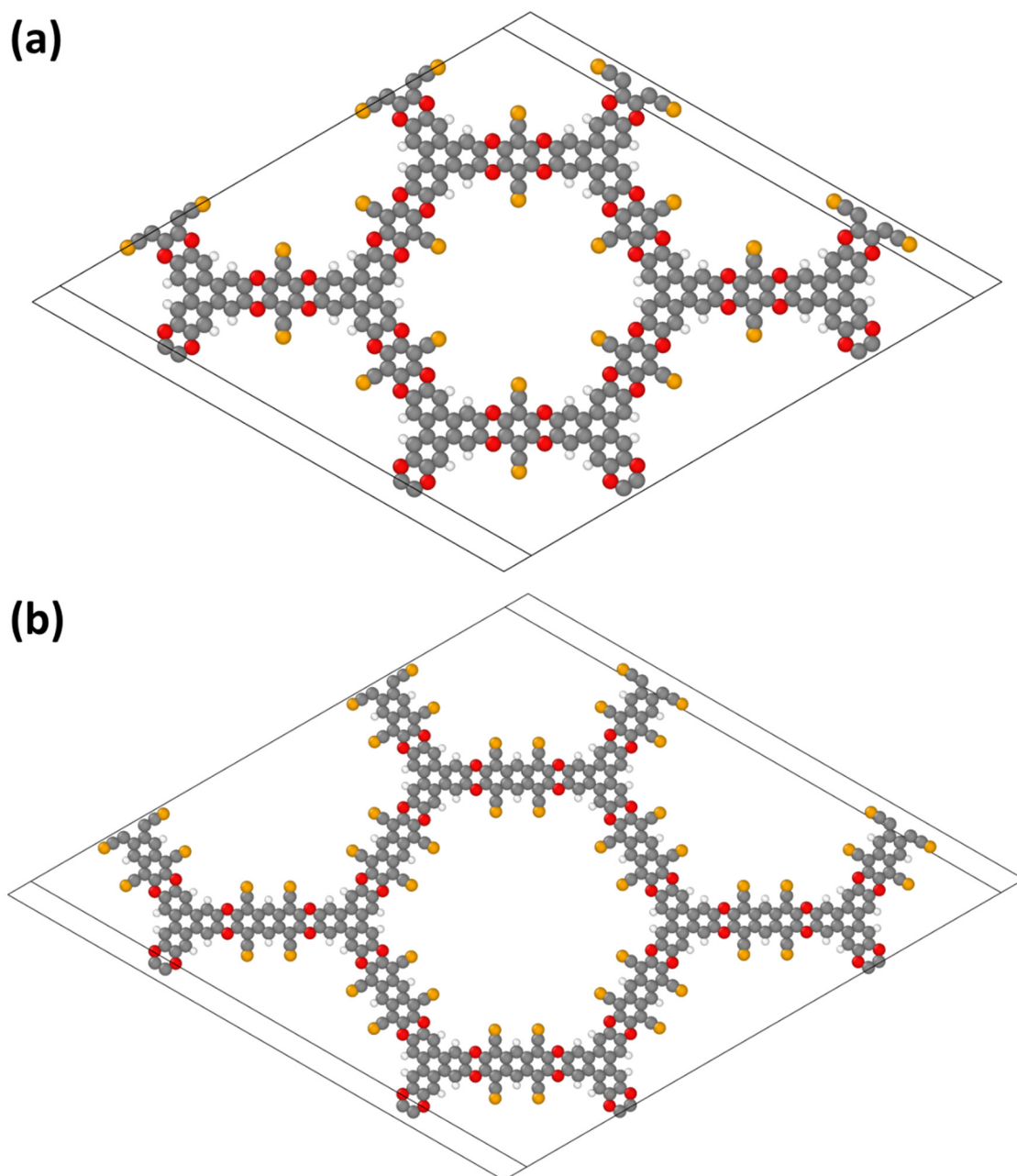


Figure S16:  $2 \times 2 \times 1$  supercells of the DFT-optimized structures of CPAE-CN (a) and a conceptually related COF with elongated linkers bearing twice the number of polar -CN substituents, referred to as COF-2CN. (colour code – grey: C orange: N, red: O; white: H; structures plotted using OVITO<sup>44</sup>).

The shifts in electrostatic energy for an electron in the centre of the pore are similar for both systems ( $\Delta E_{\text{pore}} = 0.93$  eV for CPAE-CN and  $\Delta E_{\text{pore}} = 0.86$  eV for COF-2CN). The slip between adjacent layers is only marginally different in the two systems (the angle between  $\mathbf{a}_3$  vector and  $(\mathbf{a}_1, \mathbf{a}_2)$  plane amounts to  $41.1^\circ$  vs.  $42.7^\circ$  in the two systems). This, on electrostatic grounds would result in a decrease of  $\Delta E_{\text{pore}}$  by only 2.5% in COF-2CN. Thus, the somewhat smaller value of  $\Delta E_{\text{pore}}$  in COF-2CN despite the somewhat increased dipole density must be attributed to a reduced dipole per -CN group in the case in which four polar substituents are attached to the same  $\pi$ -conjugated fragment (i.e., in COF-2CN).

## S7. Molecules adsorbed in COF pores

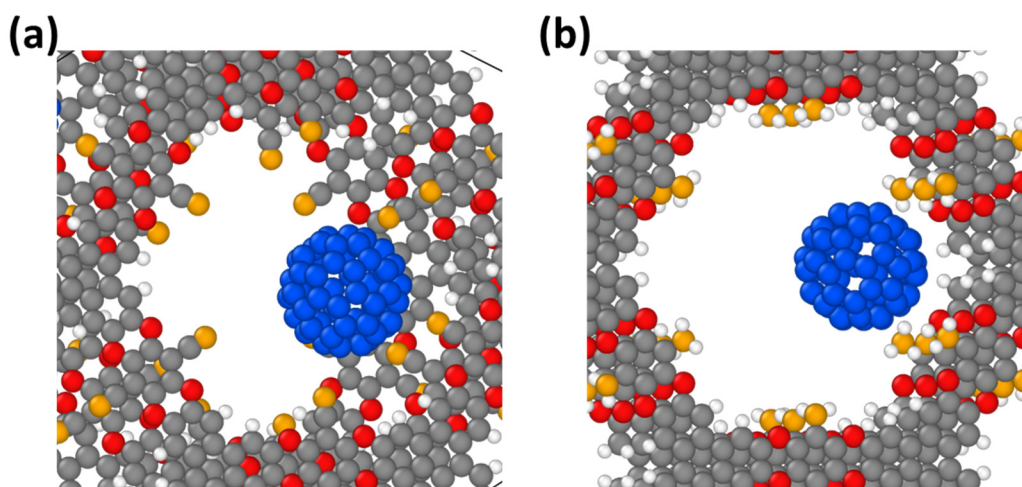


Figure S17: DFT-optimized structures of one  $C_{60}$  molecule per three COF layers in CPAE-CN (a) and CPAE-NH<sub>2</sub> (b). These geometries have been fully optimized including a unit-cell optimization. Due to the huge size of the unit cell, an intermediate basis set has been used and the convergence criterion for the forces has been doubled compared to the simulations of all structures not containing guest molecules (see also section S2) (colour code – grey: C orange: N, red: O; white: H, in the COF; blue: C in the  $C_{60}$  molecule; structures plotted using OVITO<sup>44</sup>).

## References

- 1 E. Zojer, Nano Lett., 2023, **23**, 3558–3564.
- 2 A. Stukowski, Modelling and Simulation in Materials Science and Engineering, 2010, **18**, 015012.

3 K. Momma and F. Izumi, *J Appl Cryst*, 2011, **44**, 1272–1276.